Adaptive Sliding Mode Control Strategy for Horizontal Vibration of High-speed Elevator Based on Model Identification

Li Li, Hua Li, Tichang Jia and Chen Chen

School of Mechanical and Electrical Engineering, Shandong Jianzhu University, Jinan 250101, China.
E-mail: lili0531@sdjzu.edu.cn

(Received 11 May 2023; accepted 12 August 2023)

The transverse vibration equation of a high-speed elevator car system is established to address the problem of passenger comfort due to transverse vibration caused by the unevenness of guide rails. The Hankel-Toeplitz model of transverse vibration is derived by considering the excitation-response hysteresis phenomenon. The least-squares method is used to identify the model parameters of the car system by combining the measured vibration acceleration data of the high-speed elevator. Then, the model's accuracy is verified by comparing the modeled response with the measured vibration response. Further, based on the theory of sliding mode variable structure control, an adaptive sliding mode active damping control strategy is designed for instantaneous power, and the comparative analysis of vibration acceleration and displacement of the car system under sliding mode control under light and heavy load conditions and different control strategies is carried out by MATLAB to verify the feasibility and effectiveness of the proposed control strategy parameter identification model.

1. INTRODUCTION

As a car with vertical movement on the floor, the running speed of the elevator also grows with the increase of the floor. The rise of elevator running speed makes the car's vibration in the running process more and more intense, affecting the precision and life of the precision instruments inside the elevator, bringing safety hazards to the elevator, and involving the comfort of passengers. To solve the safety and comfort problems brought by the increased elevator speed, the research on the active control method of car lateral vibration has become a hotspot for high-speed elevator vibration reduction.[1–3] Compared to active control, traditional passive vibration reduction methods can only generate small damping forces to block vibration transmission for passive vibration absorption. They are usually used in low-speed elevator situations where either the frequency remains constant or the external disturbance changes are small. Therefore, for high-speed elevators with operating speeds exceeding 2.5 m/s, this vibration reduction method cannot ensure that passengers obtain good riding comfort.[4] The active vibration reduction control method is used to install an active controller based on passive vibration reduction, in the form of adding external energy to generate an active control force that can counteract the external coupling excitation of the car system, thereby suppressing the lateral vibration of the car system.[5] Due to its significant vibration reduction effect and ability to adapt to external coupling excitation, active vibration control technology has become an important method for suppressing the lateral vibration of car systems.

When studying the active control strategy of horizontal vibration, most researchers usually model the car system by simplifying the elevator system as an M-K-C system. Feng et al.[6,7] established a vibration model of the car system based on the principle of rigid body dynamics. Cao et al.[8,9] established an eight-degree-of-freedom high-speed elevator dynamics model and conducted a robust control study of the car vibration based on it. Chen et al.[10] conducted a robust control study of car vibration preservation performance based on the established six-degree-of-freedom high-speed elevator vibration model, and Zhang et al.[11] combined the linear matrix inequality method with the parallel distribution compensation method to design an adaptive gain H∞ controller to minimize the value of the vibration index. However, the above researchers adjusted the simplified model to an ideal system without hysteresis. When the car system is excited by the displacement from the rail, the vibration energy needs a certain transition time to be transferred among the car system components. Hence, the vibration response of the car system has hysteresis, and the control response of the above studies has some immediacy problems. The literature[12] studied the H∞ control strategy for the lateral vibration time lag of the car system. Still, its authors only considered the actuator's input time lag and ignored the car system's hysteresis. Hence, the control of the car vibration still has the problem of immediacy. Therefore, in this paper, after the modeling of the car system is completed, the delayed output of the car transverse vibration is derived considering the hysteresis phenomenon of the car system itself. The least squares method[13,14] is further used to identify the car vibration output model based on experimental data to obtain a car transverse vibration model closer to the actual vibration response.

Most of the car lateral vibration control strategy research is currently focused on traditional control methods, such as the literature mentioned above are robust control methods. Santo et al.[15] proposed a Ricardian optimal control strategy for SDRE, and Xue et al.[16] designed a generalized predictive PID controller to reduce the lateral vibration of elevators. These traditional control methods are usually sensitive to parameter variations and require precise modeling parameters that are often difficult to obtain directly. A few researchers are also researching intelligent active control of lateral vibration of the car system, Zhang et al.[17] designed an active car damper using a linear motor, designed a PID car lateral vibration controller with linear predictive BP network optimization, He et al.[18] developed a fuzzy neural network controller for car lateral vibration based on pneumatic-hydraulic active guide shoe. The control methods require a large amount of data calculation by the controller during implementation and may even increase the delay of the system when controlling the car vibration, making it challenging to achieve instantaneous control.

Based on the difficulties in the implementation of the above control methods, this paper adopts a sliding mode control method,[19–21] which is easy to implement and less sensitive to parameter changes, to implement active vibration damping for elevator cabs by combining the car transverse vibration model obtained from the identification, and designs a sliding mode control strategy (IM-SMC) for transverse car vibration based on the identification model.

The main contributions of this paper are:

Firstly, the active control model of transverse vibration of a 6-degree-of-freedom (6-DOF) car system is established, and its hysteresis characteristics are described to obtain the model of a 6-DOF car system under hysteresis response. Secondly, combined with the experimental data of the real ladder, the least-squares method is applied to identify the parameters of the lateral vibration dynamics model of the 6-DOF car system under hysteresis response and the output identification model of the car system is obtained. Finally, a sliding mode active vibration suppression control strategy (IM-SMC) based on the hysteresis-identified lateral vibration model of the car system is designed and its stability is verified.

The rest of the paper is organized as follows: in Section IV, the numerical simulation results of the proposed IM-SMC control strategy are analysed under different loading conditions and different control strategies, and the proposed IM-SMC control has good vibration suppression performance. The proposed IM-SMC control has good vibration suppression performance. Finally, in Section V, the conclusion and outlook are given.

2. MODELING AND DERIVATION OF TRANSVERSE VIBRATION DYNAMICS OF HIGH-SPEED

2.1. Car System Transverse Vibration Dynamics Modeling

In the study of this paper, only the lateral vibration of a high-speed elevator under the excitation of a guide rail was considered, so the elevator components other than the car system and guide system were ignored in the modeling. In the actual elevator structure, vibration-damping rubber pads between the car and car frame can attenuate the vertical vibration transmitted to the car system. However, in the horizontal direction, because the gap between the car and frame is minimal, the vibration attenuation effect of the vibration-damping rubber in the horizontal direction will be significantly reduced. as the mass-spring-damping system shown in Figure 1.

Combine the horizontal vibration model of the car shown in Fig. 1, where the mass of the car system was mc, the rotational inertia was I_c, and the mass of the guide shoe was m_r; l_1 was the linear distance from the top guide shoe to the center of mass of the car, and l_2 was the distance from the bottom guide shoe to the center of mass of the car, assume that the contact stiffness and contact damping of each guide shoe roller and the same parts were the same, and the contact stiffness and contact damping of the guide shoe roller and the guide rail were k_2 and c_2, respectively; this system had the horizontal translation of the car x_c, the rotation around the center of mass θ_c; and the flat contact stiffness and contact damping of the four guide shoes and the car frame were k_1 and c_1, respectively; this system had the literal translation x_c of the car and the rotation θ_c around the center of mass, and the translation $x_i (i = 1, 2, 3, 4)$ of the four guide shoes, with a total of 6 degrees of freedom.

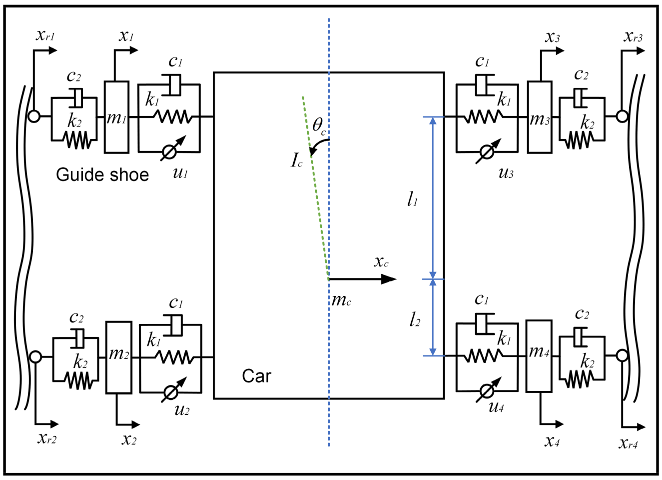

Figure 1. Car-rail coupling system dynamics model.

The relationship between the horizontal displacement at the connection of the car body and the guide shoe is as follows:

$$\begin{cases} x_{s1} = x_c - l_1 \tan\theta \approx x_c - l_1\theta \\ x_{s2} = x_c + l_2 \tan\theta \approx x_c + l_2\theta \\ x_{s3} = x_c + l_1 \tan\theta \approx x_c + l_1\theta \\ x_{s4} = x_c - l_2 \tan\theta \approx x_c - l_2\theta \end{cases}. \tag{1}$$

The transverse vibration dynamics equation of the car system is:

$$\begin{cases} m_c\ddot{x}_c = -4k_1x_c + 2k_1(l_1 - l_2)\theta \\ +k_1(x_1 + x_2 + x_3 + x_4) - 4c_1\dot{x}_c + 2c_1(l_1 - l_2)\dot{\theta} \\ +c_1(\dot{x}_1 + \dot{x}_2 + \dot{x}_3 + \dot{x}_4) + u_1 + u_2 + u_3 + u_4 \\ I_c\ddot{\theta}_c = 2k_1(l_1 - l_2)x_c - 2k_1(l_1^2 + l_2^2)\theta \\ +l_1k_1(x_1 + x_3) - l_2k_1(x_2 + x_4) + 2c_1(l_1 - l_2)\dot{x}_c \\ -2c_1(l_1^2 + l_2^2)\dot{\theta} + l_1c_1(\dot{x}_1 + \dot{x}_3) \\ -l_2c_1(\dot{x}_2 + \dot{x}_4) - l_1(u_1 + u_3) + l_2(u_2 + u_4) \\ m_1\ddot{x}_1 = k_1(x_1 - x_c + l_1\theta) + c_1\left(\dot{x}_1 - \dot{x}_c + l_1\dot{\theta}\right) \\ +k_2(x_{r1} - x_1) + c_2(\dot{x}_{r1} - \dot{x}_1) - u_1 \\ m_1\ddot{x}_2 = k_1(x_2 - x_c - l_2\theta) + c_1\left(\dot{x}_2 - \dot{x}_c - l_2\dot{\theta}\right) \\ +k_2(x_{r2} - x_2) + c_2(\dot{x}_{r2} - \dot{x}_2) - u_2 \\ m_1\ddot{x}_3 = k_1(x_3 - x_c - l_1\theta) + c_1\left(\dot{x}_3 - \dot{x}_c - l_1\dot{\theta}\right) \\ +k_2(x_{r3} - x_3) + c_2(\dot{x}_{r3} - \dot{x}_3) - u_3 \\ m_1\ddot{x}_4 = k_1(x_4 - x_c + l_2\theta) + c_1\left(\dot{x}_4 - \dot{x}_c + l_2\dot{\theta}\right) \\ +k_2(x_{r4} - x_4) + c_2(\dot{x}_{r4} - \dot{x}_4) - u_4 \end{cases}. \tag{2}$$

From Equation (2), the differential equation of motion for this system in 6 degrees of freedom can be obtained as follows:

$$\boldsymbol{M\ddot{Y}} + \boldsymbol{C\dot{Y}} + \boldsymbol{KY} = \boldsymbol{F}(t), \tag{3}$$

$$\boldsymbol{M} = \text{diag}\left[m_c, I_c, m_{r1}, m_{r2}, m_{r3}, m_{r4}\right];$$
$$\boldsymbol{Y} = \left[x_c, \theta_c, x_1, x_2, x_3, x_4\right]^T;$$
$$\boldsymbol{F}(t) = \begin{bmatrix} \sum_{i=1}^{4} u_i \\ u_1 L_1 - u_2 L_2 + u_3 L_1 - u_4 L_2 \\ k_2 x_1 + c_2 \dot{x}_1 - u_1 \\ k_2 x_2 + c_2 \dot{x}_2 - u_2 \\ k_2 x_3 + c_2 \dot{x}_3 - u_3 \\ k_2 x_4 + c_2 \dot{x}_4 - u_4 \end{bmatrix};$$
$$\boldsymbol{K} = \begin{bmatrix} 4k_1 & -2k_1(l_2 - l_1) & -k_1 & -k_1 & -k_1 & -k_1 \\ -2k_1(l_1 - l_2) & 2k_1\left({l_1}^2 + {l_2}^2\right) & -k_1 l_1 & k_1 l_2 & -k_1 l_1 & k_1 l_2 \\ k_1 & -k_1 l_1 & (k_2 - k_1) & 0 & 0 & 0 \\ k_1 & k_1 l_2 & 0 & (k_2 - k_1) & 0 & 0 \\ k_1 & -k_1 l_1 & 0 & 0 & (k_2 - k_1) & 0 \\ k_1 & k_1 l_2 & 0 & 0 & 0 & (k_2 - k_1) \end{bmatrix};$$
$$\boldsymbol{C} = \begin{bmatrix} 4c_1 & -2c_1(l_2 - l_1) & -c_1 & -c_1 & -c_1 & -c_1 \\ -2c_1(l_1 - l_2) & 2c_1\left({l_1}^2 + {l_2}^2\right) & -c_1 l_1 & c_1 l_2 & -c_1 l_1 & c_1 l_2 \\ c_1 & -c_1 l_1 & (c_2 - c_1) & 0 & 0 & 0 \\ c_1 & c_1 l_2 & 0 & (c_2 - c_1) & 0 & 0 \\ c_1 & -c_1 l_1 & 0 & 0 & (c_2 - c_1) & 0 \\ c_1 & c_1 l_2 & 0 & 0 & 0 & (c_2 - c_1) \end{bmatrix}.$$

where $\boldsymbol{M}$ denoted the mass matrix, $\boldsymbol{C}$ represented the damping matrix, K indicated the stiffness matrix, $\boldsymbol{F(t)}$ denoted the external excitation matrix, $\ddot{\boldsymbol{Y}}$, $\dot{\boldsymbol{Y}}$, $\boldsymbol{Y}$ were the vibration acceleration matrix, vibration velocity matrix, and vibration displacement matrix, respectively (see the equations on the top of this page).

2.2. Description of the Lateral Vibration Hysteresis Response of the Car System

For the elevator car horizontal vibration dynamics Equation (2) constructed in 2.1, the state variables were selected as: $\boldsymbol{X} = \left[x_c, \dot{x}_c, \theta_c, \dot{\theta}_c, x_1, \dot{x}_1, x_2, \dot{x}_2, x_3, \dot{x}_3, x_4, \dot{x}_4\right]^T$.

Output variables: $\boldsymbol{Y} = \left[x_c, \theta_c, \ddot{x}_c, \ddot{\theta}_c\right]^T$

Control variables: $\boldsymbol{f} = \left[u_1, u_2, u_3, u_4\right]^T$

Translating this into a state space form as:

$$\begin{aligned} \dot{\boldsymbol{X}} &= \boldsymbol{AX} + \boldsymbol{Bf}(t); \\ \boldsymbol{Y} &= \boldsymbol{CX} + \boldsymbol{Df}(t). \end{aligned} \tag{4}$$

To obtain a mathematical model that is more consistent with the elevator vibration state, this subsection first ignores the assumption that the sampling time is ΔT and discretizes the horizontal vibration state space model (4) of the car system that is currently $t = k\Delta T$ to obtain:

$$\boldsymbol{X}(k+1) = \boldsymbol{AX}(k) + \boldsymbol{B}_1\boldsymbol{f}(k)\boldsymbol{Y}(k) = \boldsymbol{CX}(k) + \boldsymbol{D}_1\boldsymbol{f}(k). \tag{5}$$

There is a delay in the vibration response of the car system after the car system is excited by the rail. Assuming that the hysteresis step of horizontal vibration is p, the discrete state space model of horizontal car vibration can be rewritten as:

$$\begin{aligned} \boldsymbol{X}(k+p) =& \boldsymbol{A}^p\boldsymbol{X}(k) + \boldsymbol{B}_p\boldsymbol{f}_p(k)\boldsymbol{Y}_p(k) \\ =& \boldsymbol{C}_p\boldsymbol{X}(k) + \boldsymbol{D}_p\boldsymbol{f}_p(k). \end{aligned} \tag{6}$$

Where $f_p(k)$ and $Y_p(k)$ denoted the input and output vectors of the system, respectively, B_p denoted the controllable metric matrix of the system, C_p denoted the observable metric matrix of the system, and D_p was the Toelipiz matrix of the Markov parameters of the system.

$$\boldsymbol{f}_p(k) = \begin{bmatrix} \boldsymbol{f}(k) \\ \boldsymbol{f}(k+1) \\ \dots \\ \boldsymbol{f}(k+p-1) \end{bmatrix}; \boldsymbol{Y}_p(k) = \begin{bmatrix} \boldsymbol{Y}(k) \\ \mathbf{Y}(k+1) \\ \dots \\ \boldsymbol{Y}(k+p-1) \end{bmatrix};$$
$$\boldsymbol{B}_p = \left[\boldsymbol{A}^{p-1}\boldsymbol{B}, \boldsymbol{A}^{p-2}\boldsymbol{B}, \dots, \boldsymbol{AB}, \boldsymbol{B}\right];$$
$$\boldsymbol{C}_p = \left[\boldsymbol{C}^T, (\boldsymbol{CA})^T, (\boldsymbol{CA}^2)^T, \dots, (\boldsymbol{CA}^{P-1})^T\right];$$
$$\boldsymbol{D}_p = \begin{bmatrix} \boldsymbol{D} & \boldsymbol{0} & \dots & \boldsymbol{0} \\ \boldsymbol{CB} & \boldsymbol{D} & \dots & \boldsymbol{0} \\ \dots & \dots & \dots & \boldsymbol{0} \\ \boldsymbol{CA^{p-2}B} & \boldsymbol{CA^{p-3}B} & \dots & \boldsymbol{D} \end{bmatrix}.$$

If the dimensionality of the controllable metric matrix of the system and the observable metric matrix of the system $pm > 2n$, there exists a matrix M satisfying:

$$\boldsymbol{A}^p + \boldsymbol{MC}_P = \boldsymbol{0}. \tag{7}$$

Bringing Equation (7) into Equation (6) yields,

$$\begin{aligned} \boldsymbol{Y}_p(k) =& \boldsymbol{C}_p\left(\boldsymbol{B}_p + \boldsymbol{MD}_P\right)\boldsymbol{f}_P(k-p) - \\ & \boldsymbol{C}_p\boldsymbol{MY}_p(k-p) + \boldsymbol{D}_p\boldsymbol{f}_p(k). \end{aligned} \tag{8}$$

Let, $\boldsymbol{\Theta} = \boldsymbol{C}_p\left(\boldsymbol{B}_p + \boldsymbol{MD}_P\right), \boldsymbol{\Xi} = -\boldsymbol{C}_p\boldsymbol{M}$.

Then the output expression can be further rewritten as:

$$\boldsymbol{Y}_p(k) = \begin{bmatrix} \boldsymbol{\Theta} & \boldsymbol{\Xi} & \boldsymbol{D}_p \end{bmatrix} \begin{bmatrix} \boldsymbol{f}_p(k-p) \\ \boldsymbol{Y}_p(k-p) \\ \boldsymbol{f}_p(k) \end{bmatrix}. \tag{9}$$

3. CAR SYSTEM HYSTERESIS RESPONSE MODEL IDENTIFICATION AND EXPERIMENTAL VALIDATION

3.1. Car Transverse Vibration Parameter Matrix Least Squares Method Identification

To control the horizontal vibration of the car, it was necessary to obtain a more accurate transverse vibration response first. According to Equation (9), the transverse vibration response of the car was related to the parameter matrices of $\boldsymbol{\Theta}$, $\boldsymbol{\Xi}$, and $\boldsymbol{D}_p$. To obtain the parameters of $\boldsymbol{\Theta}$, $\boldsymbol{\Xi}$, and $\boldsymbol{D}_p$ matrices accurately, the least squares method was used to identify the parameters in this subsection.[13,14]

For the car transverse vibration output expression (10), let:

$$\boldsymbol{\theta} = \begin{bmatrix} \boldsymbol{\Theta} & \boldsymbol{\Xi} & \boldsymbol{D}_p \end{bmatrix} \boldsymbol{u}_p(k) = \begin{bmatrix} \boldsymbol{f}_p(k-p) \\ \boldsymbol{Y}_p(k-p) \\ \boldsymbol{f}_p(k) \end{bmatrix}. \tag{10}$$

Get:

$$\boldsymbol{Y}_p(k) = \boldsymbol{\theta}\boldsymbol{u}_p(k); \tag{11}$$

where $\boldsymbol{\Theta}$ was the matrix of parameters to be identified.

The least squares method identified the specificp arameters of the system by minimizing the sum of squares of the observation errors. In the expression for the horizontal vibration output of the car, the parameter identification matrix is assumed to be, then for the kth observation, the estimated result is:

$$\widehat{\boldsymbol{Y}}_p(k) = \widehat{\boldsymbol{\theta}}\boldsymbol{u}_p(k). \tag{12}$$

Then the actual output and the estimated output residuals are:

$$\boldsymbol{\Delta}(k) = \boldsymbol{Y}_p(k) - \widehat{\boldsymbol{Y}}_p(k) = \boldsymbol{Y}_p(k) - \widehat{\boldsymbol{\theta}}\boldsymbol{u}_p(k). \tag{13}$$

In L observations, the observation error sum-of-squares index is taken as:

$$J = \sum_{k=1}^{L} \boldsymbol{\Delta}^2(k) = \sum_{k=1}^{L} \left[\boldsymbol{Y}_p(k) - \widehat{\boldsymbol{\theta}}\boldsymbol{u}_p(k) \right]^2 = \boldsymbol{Y}_p^T \boldsymbol{Y} - 2\boldsymbol{Y}_p^T \widehat{\boldsymbol{\theta}}^T \boldsymbol{u}_p + \boldsymbol{u}_p^T \widehat{\boldsymbol{\theta}}^T \widehat{\boldsymbol{\theta}} \boldsymbol{u}_p. \tag{14}$$

To obtain the minimum value of Equation (14), let the derivative of the sum of squares of observation errors be zero, denoted as $\widehat{\boldsymbol{\theta}}$, and obtain:

$$\widehat{\boldsymbol{\theta}} = \boldsymbol{Y}_p \boldsymbol{u}_p^T \left[\boldsymbol{u}_p \boldsymbol{u}_p^T \right]^{-1}. \tag{15}$$

3.2. Experimental Verification of Car Water Transverse Vibration Identification Model

To verify the accuracy of the identification method proposed in section 3.1, this sub-section takes a 4 m/s high-speed elevator as the experimental object and empirically acquires the car's horizontal vibration acceleration data.

In this acquisition experiment, the DT-4A acceleration tester was applied to collect the 4 m/s elevator car horizontal vibration acceleration in the high-speed elevator experimental tower, and the high-speed elevator experimental tower and DT-4A acceleration vibration tester are shown in Figure 2.

The specific steps of the data acquisition experiment were as follows: 1) Turn on the DT-4A vibration acceleration tester and zero its data; 2) Place the tester flat on the center of the car floor; 3) Run the elevator to the highest floor of the elevator test tower to ensure that the elevator can be maintained at the highest operating speed for a long time; 4) Import the stored elevator vibration acceleration data in the DT-4A tester into the

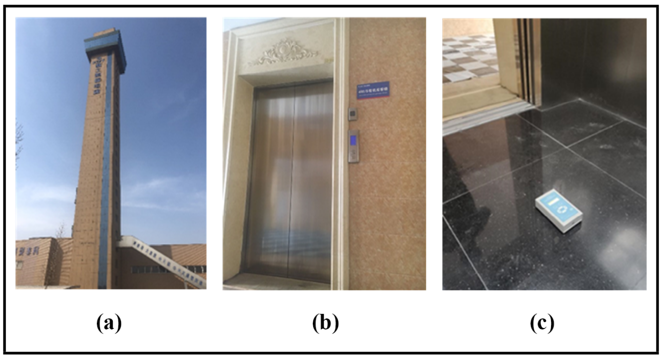

Figure 2. Experimental tools for actual data acquisition: (a) High-speed elevator experiment tower, (b) 4 m/s high-speed elevator, (c) DT-4A acceleration experiment instrument.

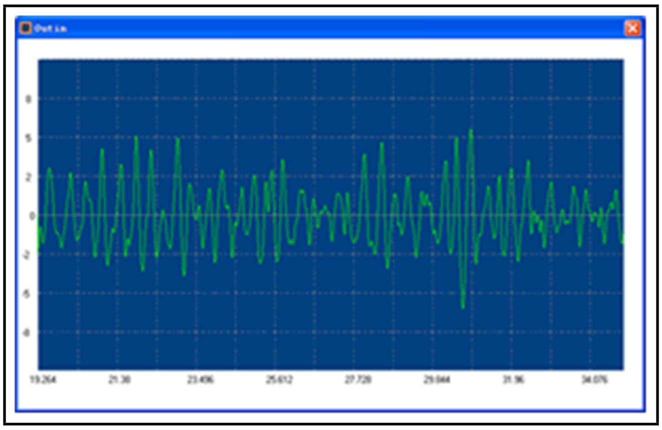

Figure 3. Measured vibration acceleration response curve of high-speed elevator car system.

Table 1. Comparison of typical numerical characteristics of simulation-measurement vibration acceleration.

Experimental method	Max	Rms	FB	FP
Tested	0.058	0.027	2-10Hz	0.0147
Identification	0.054	0.024	2-10Hz	0.0145

computer and intercept the vibration data of the highest operating speed section of the elevator. The data can be obtained through computer data processing.

The vibration response curve of the elevator in the highest speed operation stage can be obtained through computer data processing, as shown in Figure 3. Further, based on the identification model, the horizontal vibration response of the car body is solved numerically to obtain the vibration response curve, as shown in Fig. 4.

The vibration response of the car horizontal vibration recognition model was solved and compared with the measured vibration response of the car in time and frequency domains. The specific time-frequency domain comparison curve is shown in Figure 4. Further, the typical digital features such as maximum acceleration value (MAX), root mean square value (RMS), vibration frequency band (FB), and frequency domain vibration peak (FP) were extracted from the comparison curve, and the specific data comparison is shown in Table 1.

As can be seen from Fig. 4, under the same operating conditions, the simulation curve of the identification model can effectively fit the measured vibration data in time and frequency domains, and the numerical simulation curve had a very similar trend with the measured curve in both time and frequency

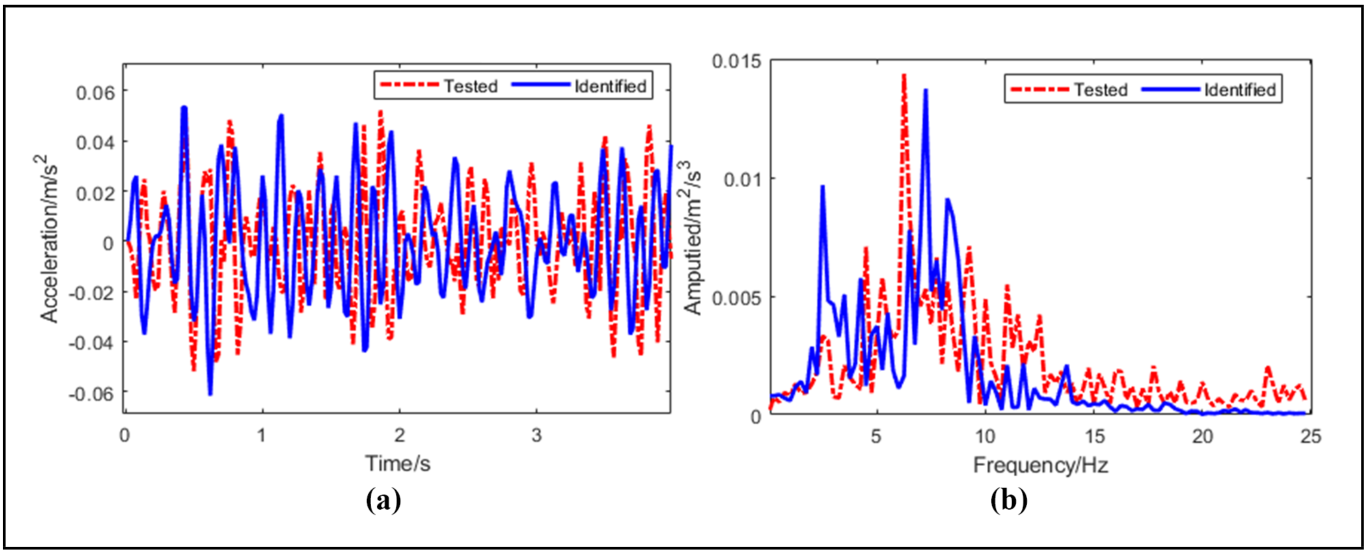

Figure 4. Simulated-measured vibration acceleration response curve of the car: (a) time domain response, (b) frequency domain response.

domains. Moreover, by comparing the digital characteristics of the car vibration, it can be seen that the difference between the RMS, MAX, FB, and FP of the recognition curve and the corresponding values of the measured data was within 10% (the reason for the formation of small-amplitude error may be because, in the experiments, the DT-4A accelerometer was placed on the car floor, which is an elastic object, and a certain degree of error will be generated, which will lead to a slight difference between simulation and experimental results), which proves that the simulation curve can effectively fit the vibration data in time and frequency domains. This proves that the identification model studied in this paper can effectively simulate the vibration response of high-speed elevator operation.

4. SLIDING MODE CONTROL STRATEGY BASED ON THE IDENTIFICATION MODEL

In Section 3.2, a hysteresis model of the car horizontal vibration dynamics was obtained by most minor squares identification, and the accuracy of the identification model was verified by comparing the measured vibration curve with the identification curve. To effectively attenuate the horizontal vibration of the car system, this subsection combines the robust sliding mode control method to suppress the horizontal vibration of the car actively.

4.1. Adaptive Sliding Mode Controller Design

For the high-speed elevator horizontal vibration dynamics model, introducing the control vector $\boldsymbol{u}_c(k) = \begin{bmatrix} u_{c1} & u_{c2} \end{bmatrix}^T$, combined with the vibration output expressions (11), (12), and (15), the car horizontal vibration state space can be further rewritten as:

$$\boldsymbol{Y}(k) = \widehat{\boldsymbol{\theta}}\boldsymbol{u}_p(k) + \boldsymbol{D}_c\boldsymbol{u}_c(k); \tag{16}$$

where $\boldsymbol{D}_c$ was the control input matrix.

The control goal of the car system was to reduce its crucial index values (such as vibration acceleration and displacement) to zero as much as possible. However, when the car's horizontal vibration acceleration and vibration velocity are zero, the car's horizontal vibration displacement is also zero. Therefore, the tracking error was set as follows:

$$\boldsymbol{e} = \begin{bmatrix} \dot{x} \\ \ddot{x} \end{bmatrix} = \boldsymbol{Y} - 0. \tag{17}$$

Then the sliding mode function can be set as follows:

$$\boldsymbol{s} = \boldsymbol{S}\int edt = \boldsymbol{S}\begin{bmatrix} x \\ \dot{x} \end{bmatrix} = \begin{bmatrix} S_1 & S_2 \\ S_3 & S_4 \end{bmatrix}\begin{bmatrix} x \\ \dot{x} \end{bmatrix} = \begin{bmatrix} S_1x + S_2\dot{x} \\ S_3x + S_4\dot{x} \end{bmatrix}. \tag{18}$$

To control the operation of the system with slight jitter, a quasi-sliding mode approach was used to design the controller, and the control law was organized as follows:

$$\boldsymbol{u}_c = -\boldsymbol{SD}^{-1}\left(\boldsymbol{S}\widehat{\boldsymbol{\theta}}\boldsymbol{u}_p(k)\right) - \boldsymbol{SD}^{-1}\left(\frac{\boldsymbol{s}(t)}{||\boldsymbol{s}(t)|| + \delta}\right). \tag{19}$$

4.2. Stability Conditions of Slide-mode Controller

Theorem: For the car horizontal vibration control system (16), there exists a sliding mode function (18) and a control law (19), which makes the system asymptotically stable.

Proof: Combining with the sliding mode function (18), the Liapunov function of the sliding mode control system can be obtained as:

$$V = \frac{1}{2}\boldsymbol{s}\boldsymbol{s}^T = \frac{1}{2}\left[(s_1x + s_2\dot{x})^2 + (s_3x + s_4\dot{x})^2\right]. \tag{20}$$

The first derivative of the Lyapunov function yields,

$$\begin{aligned}
&\dot{V} = \boldsymbol{s}^T\dot{\boldsymbol{s}} = \boldsymbol{s}^T\boldsymbol{S}\boldsymbol{e} = \boldsymbol{s}^T\boldsymbol{S}\boldsymbol{Y} = \\
&\boldsymbol{s}^T\boldsymbol{S}\left(\hat{\boldsymbol{\Theta}}\boldsymbol{u}_p(k) + \boldsymbol{D}_c\boldsymbol{u}_c(k)\right) = \boldsymbol{s}^T\hat{\boldsymbol{\Theta}}\boldsymbol{u}_p(k) + \\
&\boldsymbol{s}^T\boldsymbol{S}\boldsymbol{D}_c\boldsymbol{u}_c(k) = \boldsymbol{s}^T\boldsymbol{S}\hat{\boldsymbol{\Theta}}\boldsymbol{u}_p(k) + \boldsymbol{s}^T\boldsymbol{S}\boldsymbol{D}_c\cdot \\
&\left((-\boldsymbol{S}\boldsymbol{D}_c)^{-1}\left(\boldsymbol{S}\hat{\boldsymbol{\Theta}}\boldsymbol{u}_p(k)\right) - (\boldsymbol{S}\boldsymbol{D}_c)^{-1}\right)\left(\frac{\boldsymbol{s}(k)}{\parallel \boldsymbol{s}(k) \parallel + \delta}\right)\Big) \\
&= -\frac{\boldsymbol{s}(k)^T\boldsymbol{s}(k)}{\parallel \boldsymbol{s}(k) \parallel + \delta}.
\end{aligned} \tag{21}$$

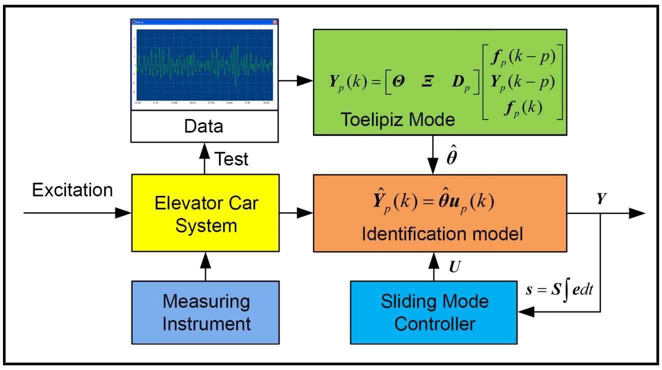

Figure 5. Flowchart of car vibration recognition model sliding mode control.

Table 2. Specific parameters of high-speed elevators.

Parameter	Value	Unit	Parameter	Value	Unit
m_c	2000	kg	c_2	134	N · s/m
I_c	4048	kg · m^2	l_1	2.00	m
k_1	3×10^5	N/m	l_2	1.50	m
c_1	920	N · s/m	m_i (i=1,2,3,4)	13	kg
k_2	6.71×10^4	N/m			

Since $\boldsymbol{s}(k)^T\boldsymbol{s}(k) > 0$, $\parallel \boldsymbol{s}(k) \parallel > 0$, it is accepted that:

$$\dot{V} = \boldsymbol{s}^T\dot{\boldsymbol{s}} = -\frac{\boldsymbol{s}(k)^T\boldsymbol{s}(k)}{\|\boldsymbol{s}(k)\| + \delta} < 0. \tag{22}$$

From Equation (22), the designed control law can satisfy both the stability of the control system and the accessibility of the sliding mode motion, and the proof is completed.

Based on the dynamics model of the high-speed elevator car system constructed in the second subsection, the flow chart of the horizontal vibration sliding mode controller of the high-speed elevator car system based on the recognition model can be obtained as shown in Fig. 5 by combining the proposed recognition method of horizontal car vibration hysteresis model and the designed adaptive sliding mode control strategy.

5. NUMERICAL SIMULATION CASE ANALYSIS

To verify the effectiveness of the designed sliding mode controller on the active suppression of horizontal vibration of the car, the Gaussian white noise excitation[22] was used to simulate the guideway unevenness excitation, and the MATLAB software was applied to the numerical simulation of the car system under the guideway unevenness excitation with different load conditions and different control strategies. In this subsection, the 4 m/s high-speed elevator will be used as the experimental object, and the specific parameters of the high-speed elevator used are shown in Table 2. The lateral vibration response characteristic curve of the car system under Gaussian white noise excitation at light load conditions is shown in Fig. 6.

From Fig. 6, it can be seen that when the car system receives the excitation effect of the guideway unevenness, it will produce serious vibration problems, which in turn affects the ride comfort of the passengers, for this reason, it is necessary to implement the active vibration suppression control of the high-speed elevator car system to attenuate its transverse vibration and to improve the operating quality and performance of the high-speed elevator.

6. NUMERICAL SIMULATION OF CONTROL PERFORMANCE UNDER DIFFERENT LOAD CONDITIONS

(1) Numerical simulation of the horizontal vibration control performance of the car system under light load conditions

To verify the effectiveness of the designed sliding mode controller for load variations during elevator operation, simulation experiments are conducted for the high-speed elevator under light load (with fewer passengers or less cargo, it is equivalent to an empty load situation) and heavy load conditions (with many passengers or cargo, equivalent to a fully loaded situation) in this subsection to verify the effectiveness of the designed controller. Firstly, the numerical simulation experiments of horizontal square vibration acceleration and vibration displacement, deflection angle, and angular acceleration at the center of mass of the car in the case of no control and sliding mode control are carried out for the car system identification model of the high-speed elevator under light load conditions. The frequency domain curves of horizontal vibration acceleration at the center of mass of the car system under light load are shown in Fig. 7, the frequency domain curves of horizontal vibration displacement at the center of mass of the car are shown in Fig. 8, the frequency domain curves of deflection angle acceleration at the center of mass of the car are shown in Fig. 9, and the frequency domain curves of deflection angle at the center of mass of the car are shown in Fig. 10.

From the time-frequency comparison curves of the critical indicators of horizontal vibration of the car system in Fig. 7, 8, 9, 10, it is evident that: in the time domain, the peaks of horizontal vibration acceleration and displacement and deflection angle at the center of mass of the car under the sliding mode control strategy are much smaller than the peaks of typical digital eigenvalues without control; and in the frequency domain, the designed sliding mode control strategy can also significantly reduce the peaks of typical digital eigenvalues in the low-frequency vibration band. In the frequency domain, the designed sliding mode control strategy can also considerably reduce the vibration peak of each distinct digital eigenvalue in the low-vibration band. To clearly represent the control effect of the designed sliding mode controller on the horizontal vibration of the car system, the typical numerical index values of vibration acceleration and displacement and deflection angle (i.e., maximum value (Max), root mean square value (Rms) and vibration peak value (FP)) in the frequency domain curve of vibration response are extracted respectively, and the specific values are shown in Table 3.

Comparing the specific data in Table 3, we can see that, compared with passive damping, in the frequency domain, the maximum value of horizontal vibration acceleration of the car system under sliding mode control is reduced by 89.4%, the root mean square value is reduced by 85.2%, the maximum value and root mean square value of horizontal vibration displacement are reduced by 83% and 79.3% respectively, and the maximum values of horizontal vibration angular acceleration and deflection angle of the car system are reduced by 80% and 73.3% respectively. The root means the square value is reduced by 77.3% and 70%, respectively. In the frequency domain, the vibration peak of horizontal vibration acceleration of the car system under sliding mode control is reduced by 90.1%, the horizontal vibration displacement is reduced by 80.8%, the

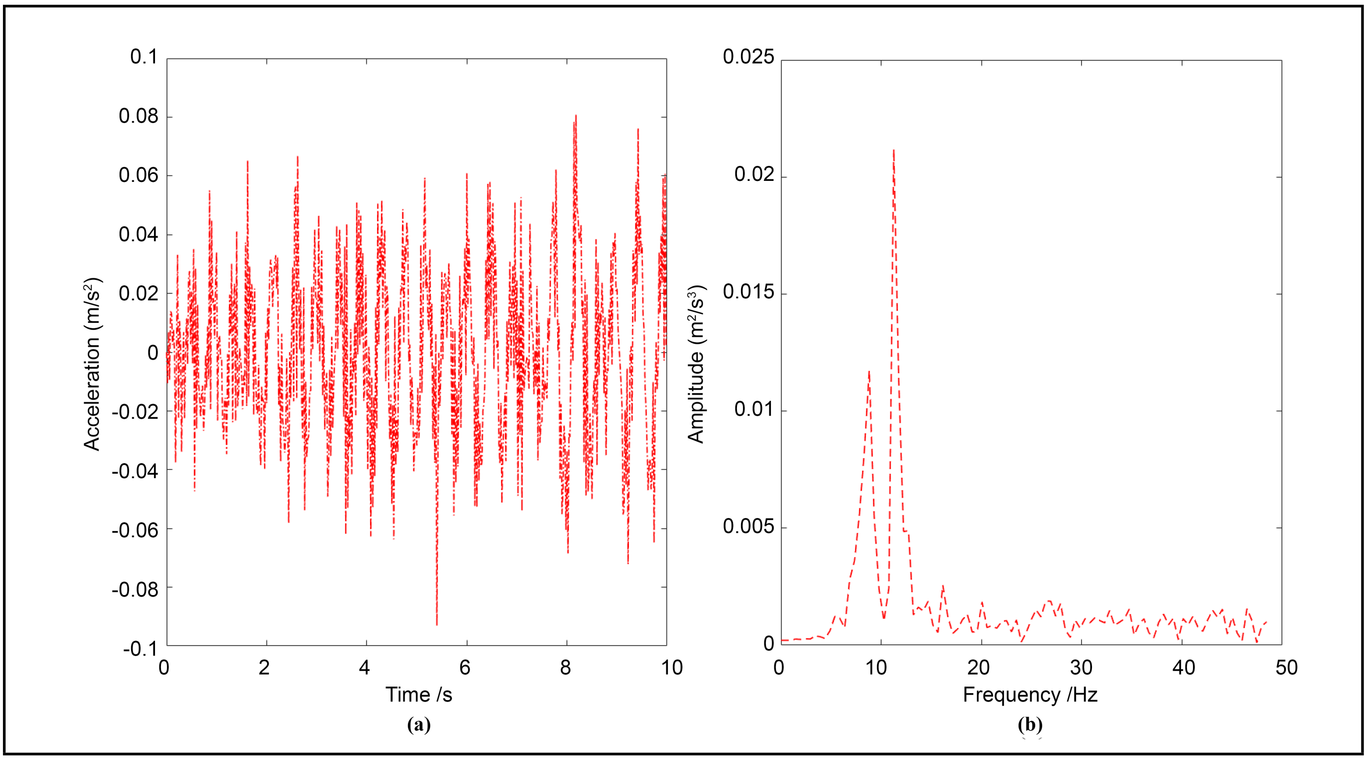

Figure 6. Characteristic curves of transverse vibration response of car system under guideway excitation.

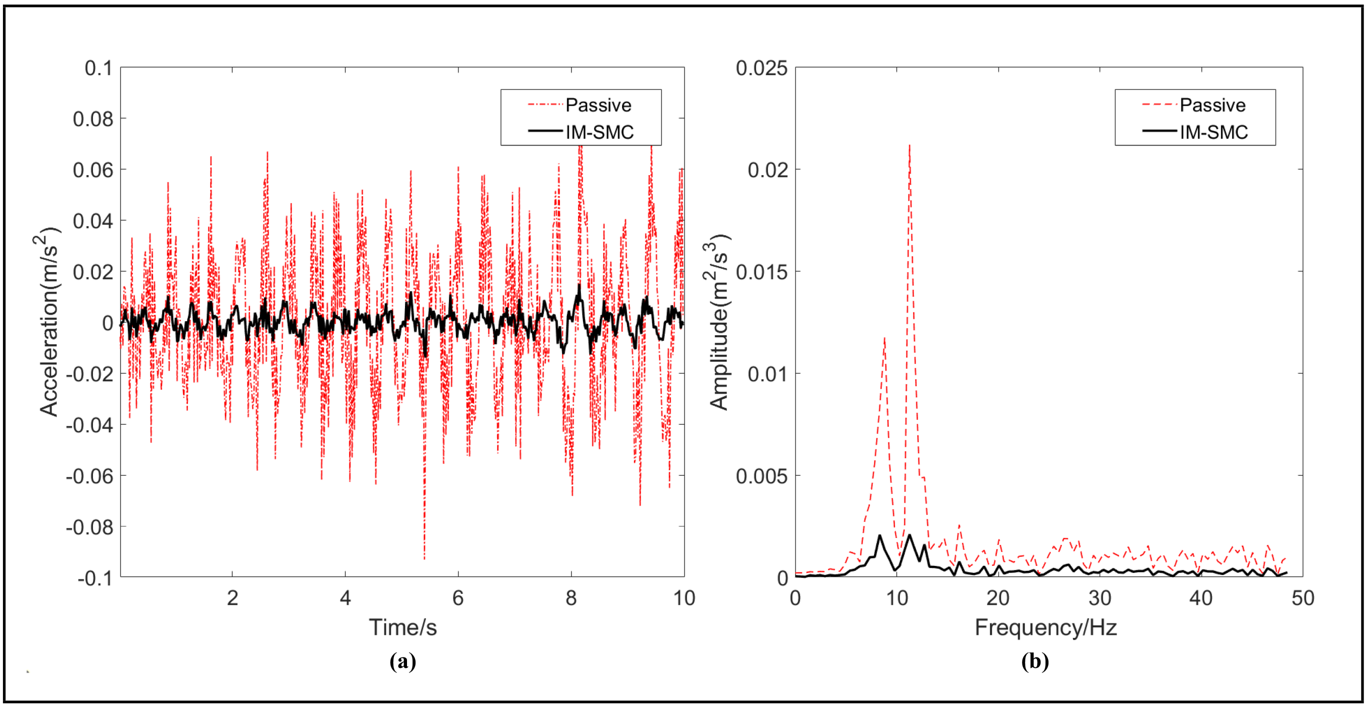

Figure 7. Vibration acceleration index curve at the center of mass of the car system: (a) time domain curve, (b) frequency domain curve.

angular acceleration is reduced by 72.2%, and the deflection angle is reduced by 72.7%.

(2) Numerical simulation of the horizontal vibration control performance of the car system under heavy load condition

Similarly, simulation experiments were conducted for the control performance of the car system identification model in the uncontrolled and sliding mode control cases under heavy loads. The horizontal vibration acceleration and displacement time-frequency domain curves at the center-of-mass position of the car under heavy load are shown in Fig. 11 and Fig. 12, respectively. The time-frequency domain curves of vibration angular acceleration and deflection angle are shown in Fig. 13 and Fig. 14, respectively. The typical numerical index values (i.e., maximum value (Max), root mean square value (Rms), and peak vibration value (FP)) of horizontal vibration of the car system in the uncontrolled and sliding mode-controlled states were extracted, respectively, and the specific values are shown in Table 4.

As can be seen in Figs. 11, 12, 13, 14, when the carload increases, the designed sliding mode control strategy can still

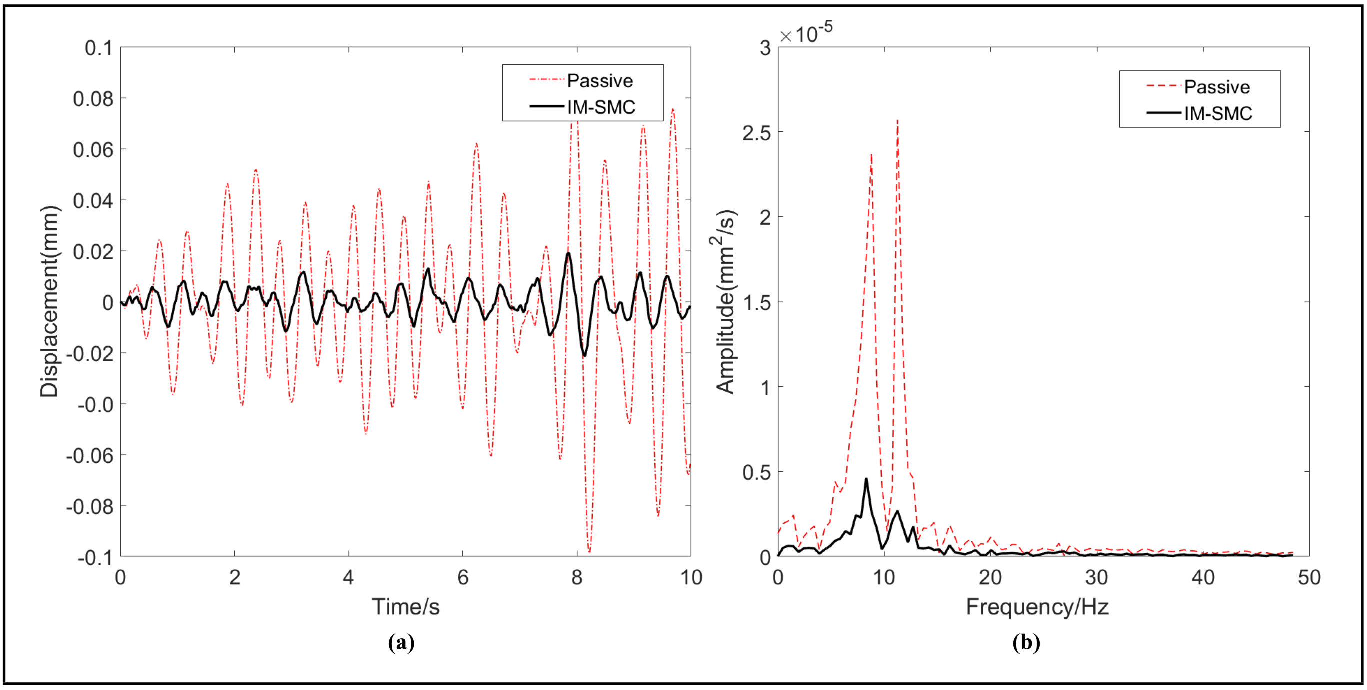

Figure 8. Vibration displacement index curve at the center of mass of the car system: (a) time domain response, (b) frequency domain response.

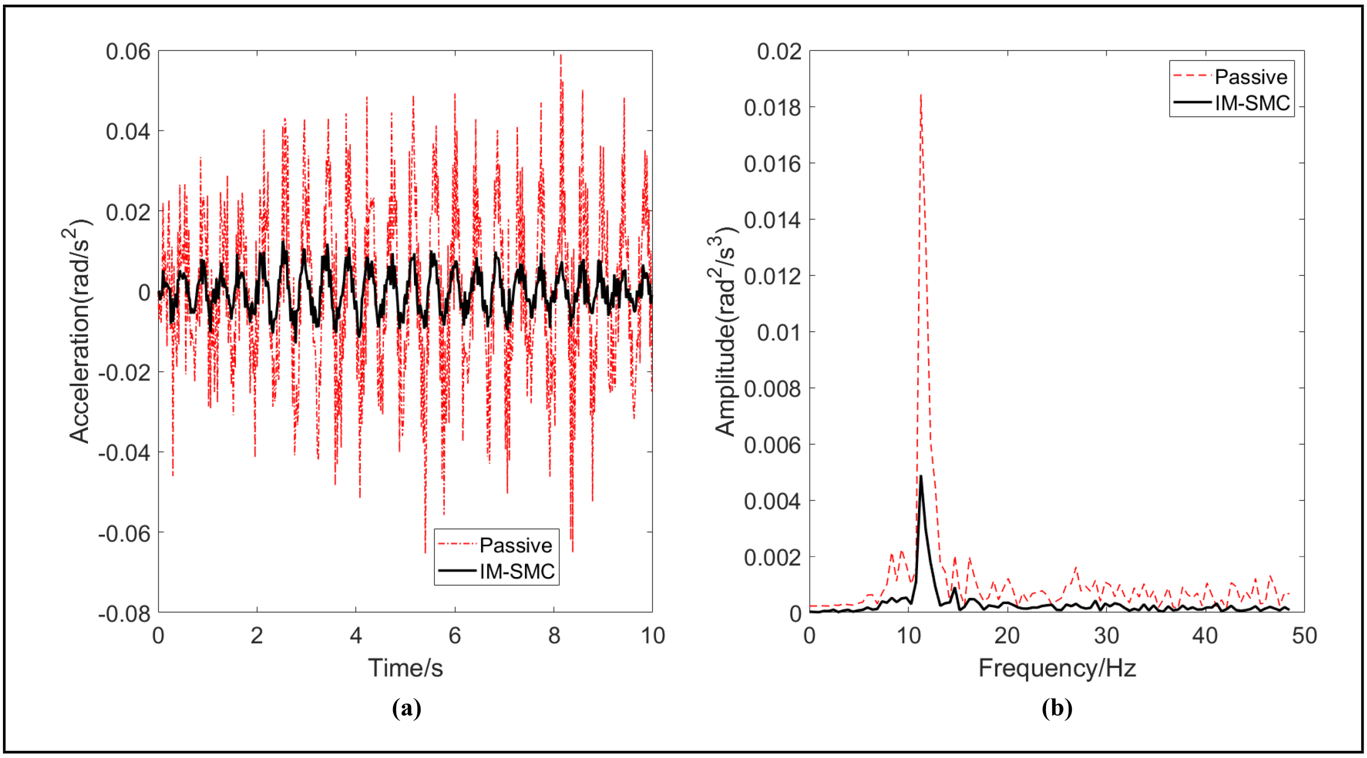

Figure 9. Frequency domain response curve when deflecting angular acceleration at the center of mass of the car system: (a) time domain curve, (b) frequency domain curve.

Table 3. Comparison of typical numerical indicators of horizontal vibration of car system under light load working condition.

Digital Indicators	Control Strategy	Max	Rms	FP
Acceleration	Passive	0.104(m/s^2)	0.027	0.022(m^2/s^3)
	IM-SMC	0.011(m/s^2) (↓89.4%)	0.004(↓85.2%)	0.002(m^2/s^3) (↓90.1%)
Displacement	Passive	0.100(mm)	0.029	0.026(mm^2/s)
	IM-SMC	0.017(mm) (↓83%)	0.006(↓79.3%)	0.005(mm^2/s) (↓80.8%)
Angular acceleration	Passive	0.065(rad/s^2)	0.022	0.018(rad^2/s^3)
	IM-SMC	0.013(rad/s^2) (↓80%)	0.005(↓77.3%)	0.005(rad^2/s^3) (↓72.2%)
Angle	Passive	0.045(rad)	0.020	0.022(rad^2/s)
	IM-SMC	0.012(rad) (↓73.3%)	0.006(↓70%)	0.006(rad^2/s) (↓72.7%)

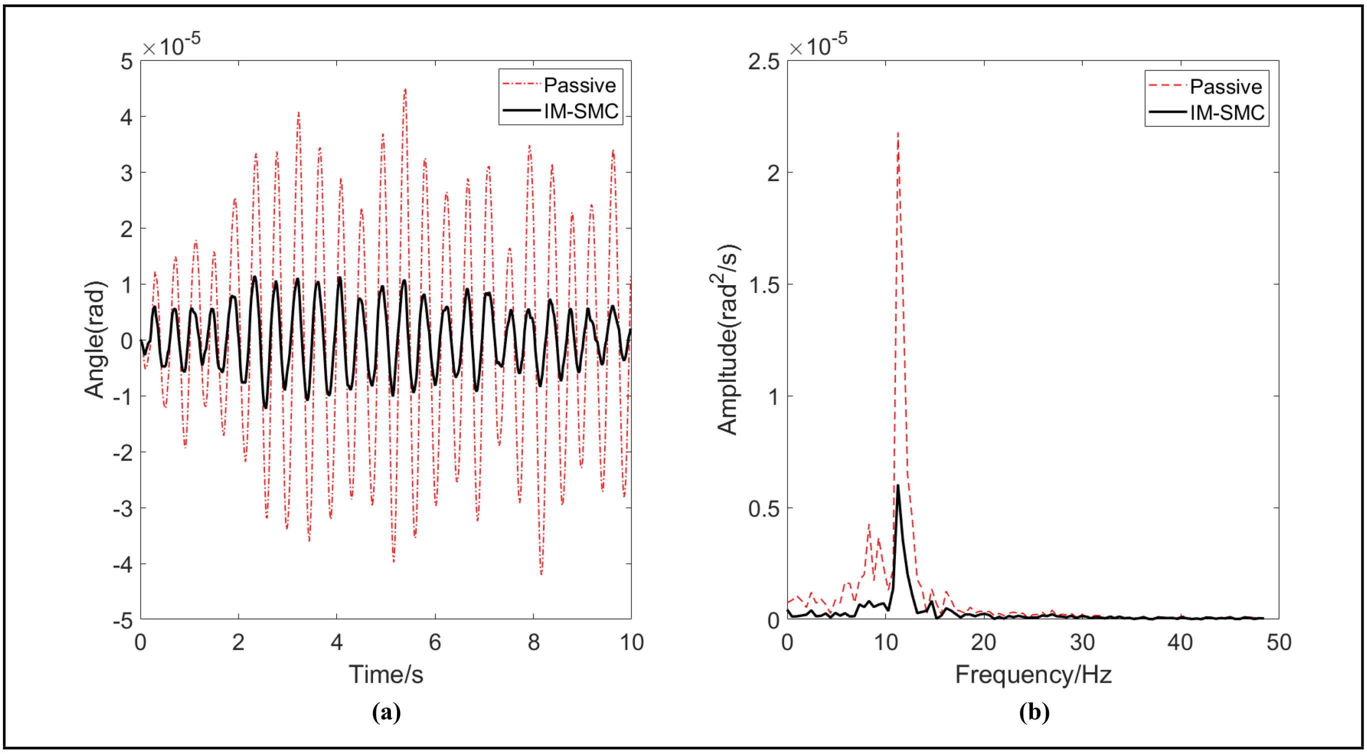

Figure 10. Frequency domain response curve at the deflection angle at the center of mass of the car system: (a) time domain curve, (b) frequency domain curve.

Table 4. Comparison of typical digital indicators of horizontal vibration of the car under heavy load working condition.

Digital Indicators	Control Strategy	Max	Rms	FP
Acceleration	Passive	0.093(m/s^2)	0.029	0.022(m^2/s^3)
	IM-SMC	0.015(m/s^2) (↓83.9%)	0.005(↓82.8%)	0.002(m^2/s^3) (↓90.1%)
Displacement	Passive	0.100(mm)	0.034	0.026(mm^2/s)
	IM-SMC	0.021(mm) (↓79%)	0.006(↓82.4%)	0.005(mm^2/s) (↓80.7%)
Angular acceleration	Passive	0.065(rad/s^2)	0.022	0.019(rad^2/s^3)
	IM-SMC	0.010 (rad/s^2) (↓84.6%)	0.003(↓86.4%)	0.001(rad^2/s^3) (↓94.7%)
Angle	Passive	0.042 (rad)	0.020	0.023 (rad^2/s)
	IM-SMC	0.008(rad) (↓81%)	0.002(↓90%)	0.002(rad^2/s) (↓91.3%)

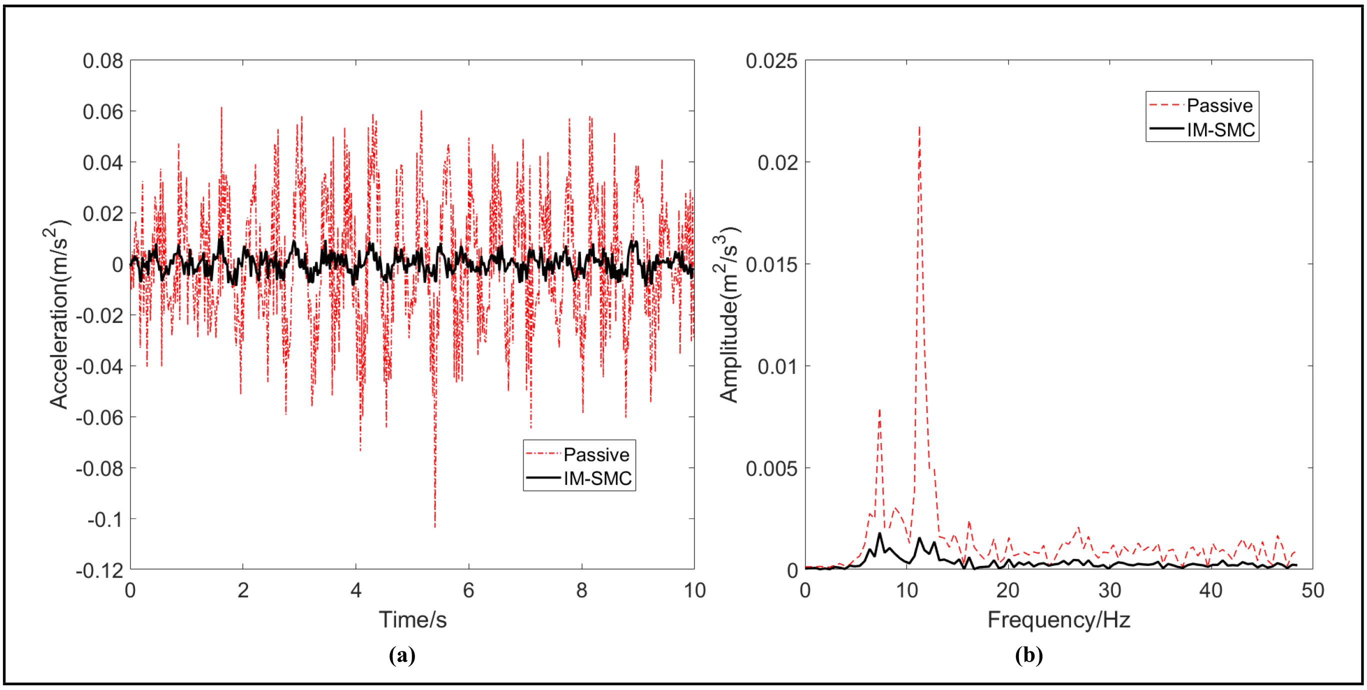

Figure 11. Horizontal vibration acceleration index time-frequency domain curve at the center of mass of the car system: (a) time domain response, (b) frequency domain response.

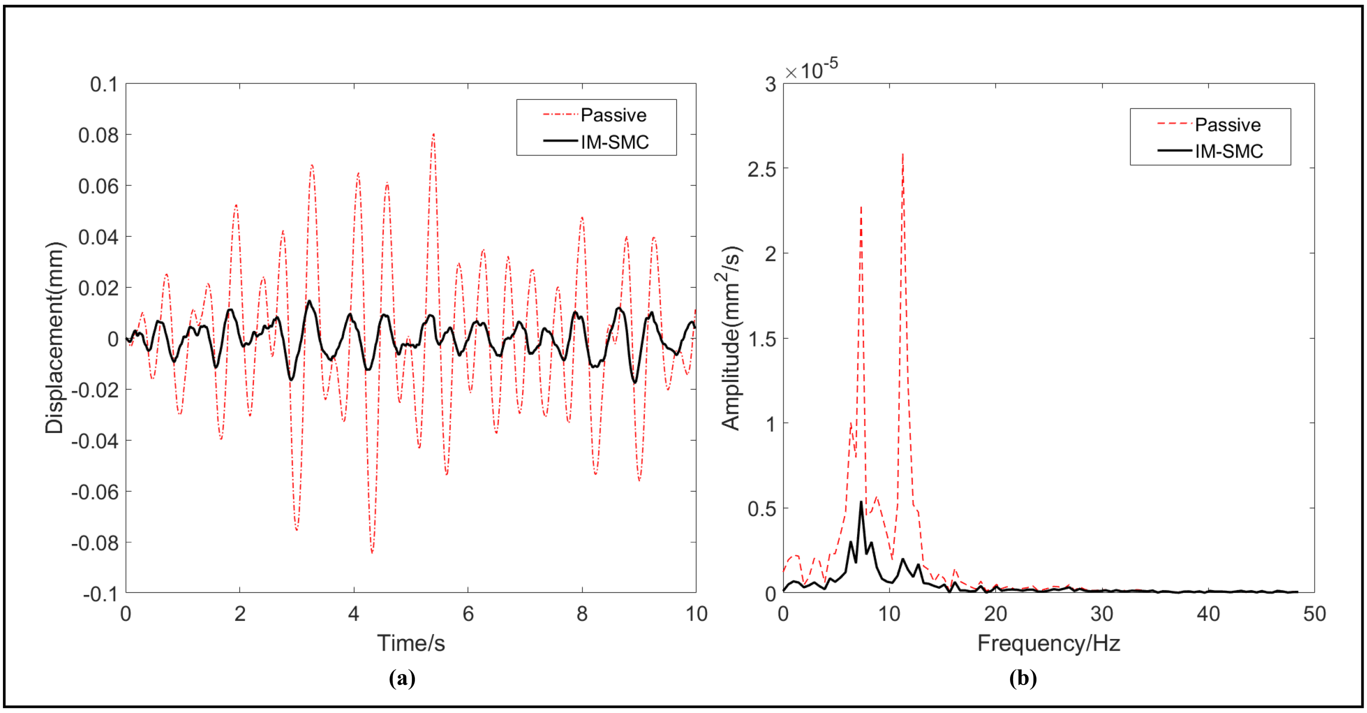

Figure 12. Horizontal vibration displacement index time-frequency domain curve at the center of mass of the car system: (a) time domain response, (b) frequency domain response.

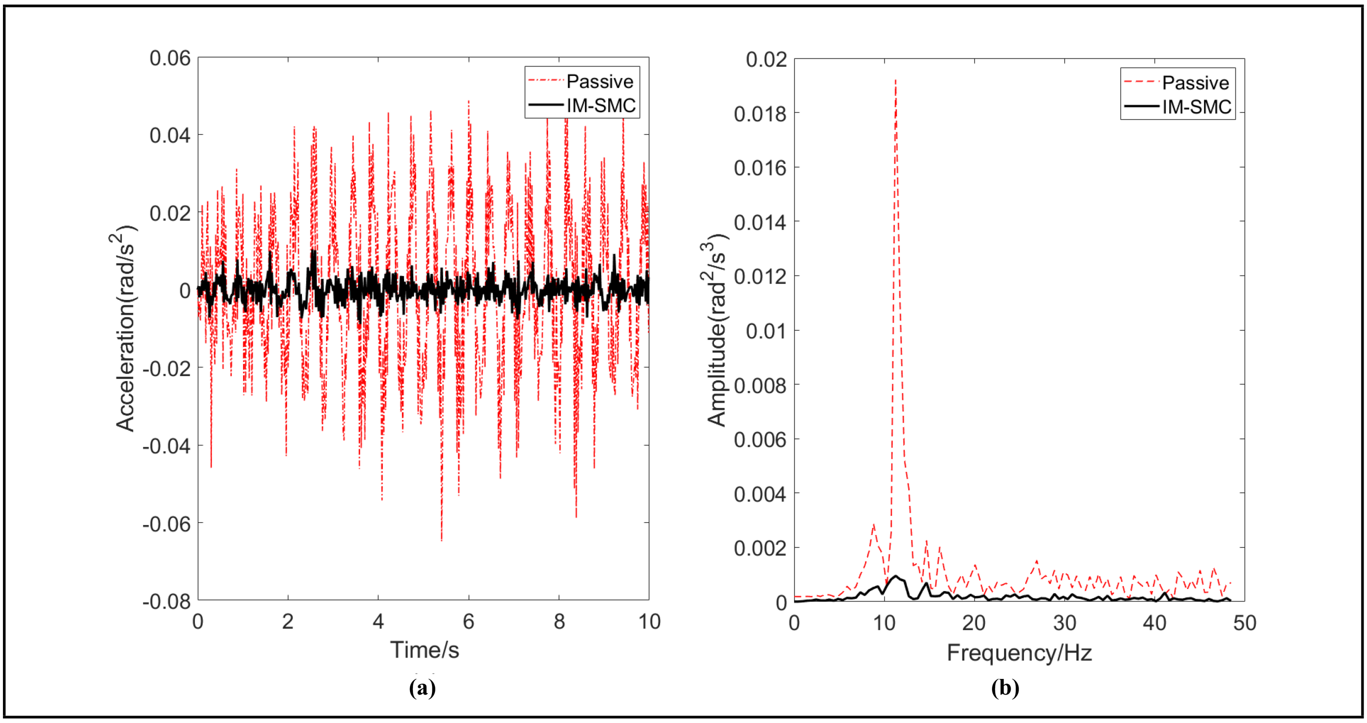

Figure 13. Time and frequency domain curves of horizontal vibration angular acceleration index at the center of mass of the car system: (a) time domain response, (b) frequency domain response.

significantly reduce the horizontal vibration of the car system with good robustness and vibration suppression performance compared with the passive control. The comparison of specific vibration indexes in Table 4 shows that compared with the passive control, the maximum value of horizontal vibration acceleration and root mean square value of the car system in the time domain are reduced by 83.9% and 82.8% respectively under the control of the sliding mode controller, and the maximum value of horizontal vibration displacement and root mean square value of the car system are reduced by 79% and 82.4% respectively under the control of the sliding mode controller, The maximum value of horizontal vibration angular acceleration and root mean square value of the car system decreased by 84.6% and 86.4% respectively under the control of the sliding mode controller, and the maximum value of horizontal vibration deflection angle and root mean square value of the car system decreased by 81% and 90% respectively under the control of the sliding mode controller; while in the frequency range, the vibration peak of each key figure of the horizontal vibration of the car system had The proposed IM-SMC control strategy

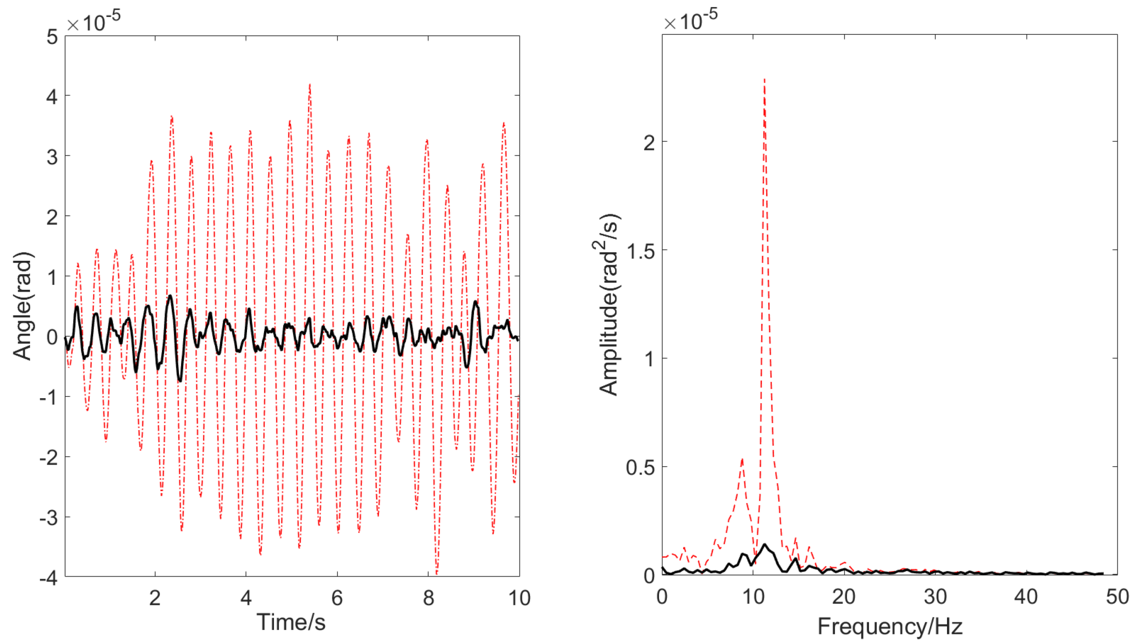

Figure 14. Frequency domain curve of horizontal vibration deflection angle indicator at the center of mass of the car system: (a) time domain response, (b) frequency domain response.

can effectively suppress the fundamental index values of horizontal vibration of the car system and significantly improve the horizontal vibration in the frequency band of 5–15 Hz.

Through the above analysis, it can be seen that the designed sliding mode control strategy can effectively reduce the horizontal vibration displacement, acceleration, and deflection angle at the center of mass of the car in both time and frequency domains under both light load and heavy load conditions based on the horizontal vibration identification model of the car system established in this paper, and all the relevant typical index values have more than 72% attenuation, indicating that the designed sliding mode controller has good control effect and vibration suppression performance. The designed sliding mode controller has a good control effect and vibration suppression performance.

7. NUMERICAL SIMULATION OF CONTROLLED PERFORMANCE WITH DIFFERENT CONTROL STRATEGIES

To further verify the effectiveness of the designed controller for active vibration damping, this subsection will apply the GA-LQR controller used in the literature[23] and the controller designed in this paper (IM-SMC) to actively control the acceleration time and frequency domain response at the center of mass of the car system together and compare the control effects.

By applying MATLAB to simulate the vibration acceleration of the established car system identification model, the time and frequency domain response curves of the horizontal vibration acceleration of the car system under the passive state, GA-LQR control, and IM-SMC control can be obtained as shown in Fig. 15, and further extract the typical numerical characteristics of the horizontal vibration acceleration and vibration displacement for comparison and analysis, whose specific values are shown in Table 5.

Table 5. Comparison of typical digital indicators of horizontal vibration of the car under different control strategies.

Digital Indicators	Control Strategy	Max	Rms
Acceleration	Passive	0.093(m/s^2)	0.029
	GA-LQR	0.045(m/s^2) (↓51.6%)	0.014(↓51.7%)
	IM-SMC	0.015(m/s^2) (↓83.9%)	0.005(↓82.8%)
Displacement	Passive	0.100(mm)	0.030
	GA-LQR	0.021(mm) (↓79%)	0.004(↓86.7%)
	IM-SMC	0.016(mm) (↓84%)	0.006(↓80%)

From the comparative analysis of the typical numerical index values of the car system under different control strategies in Table 5, it can be seen that compared with the passive state, the maximum value and root mean square value of horizontal vibration acceleration of the car system under GA-LQR control decrease by 51.6% and 51.7%, respectively, while the maximum value and root mean square value of horizontal vibration acceleration of the car system under IM-SMC control decrease by 83.9% and 82.8%, respectively, The maximum value of horizontal vibration displacement and the root mean square value of the car system under IM-SMC control decreased by 84% and 80%.

The simulation data of the vibration mentioned above index values show that the proposed IM-SMC control strategy can effectively suppress the horizontal vibration of the car system caused by the guideway excitation. The typical numerical index values of the horizontal vibration acceleration, displacement, and deflection angle of the car system are all significantly attenuated, which indicates the effectiveness of the designed control strategy for active vibration reduction.

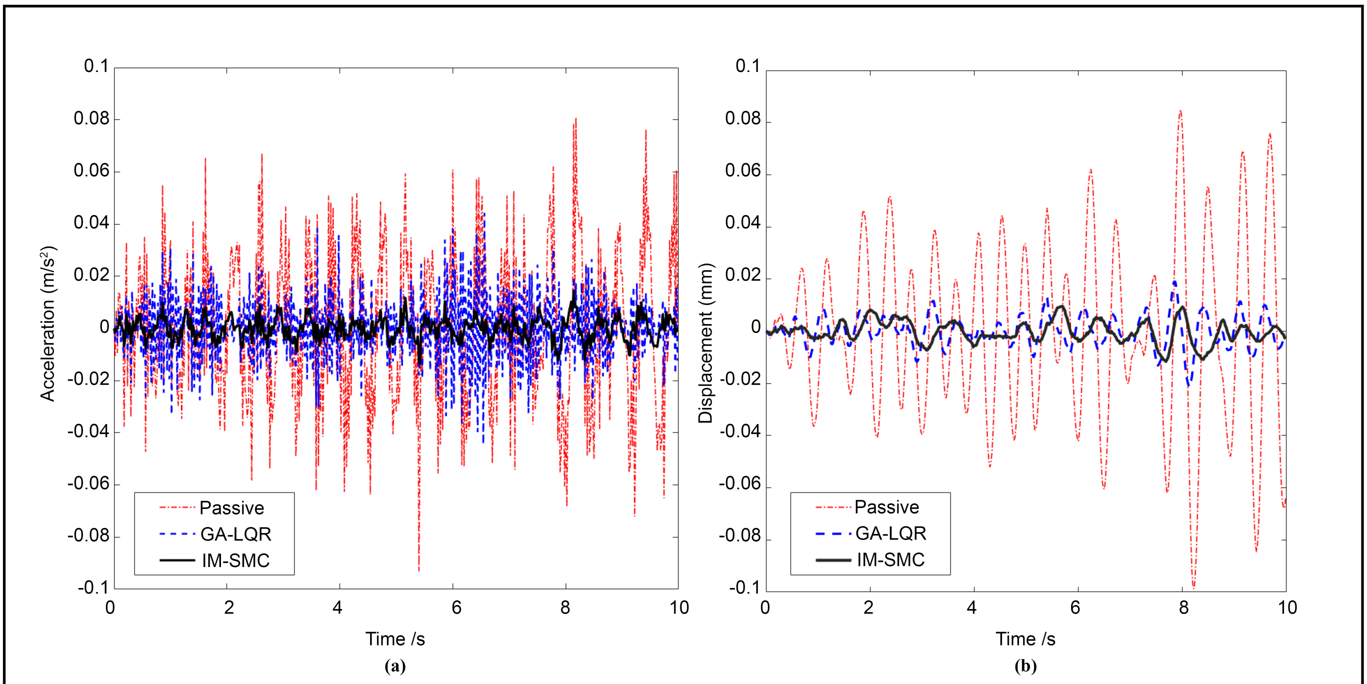

Figure 15. Frequency domain analysis curve of vibration index at the bottom center of the car: (a) vibration acceleration, (b) vibration displacement.

8. CONCLUSIONS AND FUTURE OUTLOOK

(1) In this study, a sliding mode control strategy with immediate control is designed to suppress the car's lateral vibration caused by the guideway's unevenness. Firstly, a dynamics model of the transverse vibration of a high-speed elevator car system is established. The Hankel-Toeplitz model of horizontal vibration is derived considering the excitation-response hysteresis phenomenon. The parameters of the established model are identified by combining the measured data of a 4 m/s high-speed elevator and the least squares identification method. The identification model of the car system is obtained. Further, the model is simulated and compared with the measured vibration response of the elevator, and the difference between the typical numerical index values is within 5%, which verifies the model's accuracy.

(2) Based on the proposed Hankel-Toeplitz identification model, the active vibration reduction strategy of sliding mode control based on the identification model is designed by applying the sliding mode variable structure control principle. Finally, the numerical simulation analysis of the car system under the sliding mode control strategy with different load conditions is carried out by MATLAB software, the horizontal vibration response curves of the car system are obtained, and the numerical indexes are compared with the response results under passive damping. The proposed sliding mode control strategy is verified to have a better control effect by comparing the controlled performance with that of the GA-LQR controller.

(3) In this paper, the design of the controller is carried out under ideal conditions. A variety of nonlinear coupling factors during the actual operation of the elevator can also cause lateral vibration problems in the car system. Therefore, it is necessary to further explore the influence of nonlinear factors on car vibration for more effective and precise control of transverse vibration of high-speed elevator car systems in the future.

9. ACKNOWLEDGEMENTS

This study was funded by the Shandong Province Natural Science Foundation, China (grant number ZR2021ME210), and the Shandong Province Natural Science Foundation, China (grant number ZR2021ME245). The authors are grateful for the equipment support provided by Shandong FJZY Elevator Co., Ltd. The authors sincerely thank the editors and reviewers for their insights and comments to further improve the quality of the manuscript.

REFERENCES

1. Colon, D., Cunha, A., Kaczmarczyk, S., et al. On dynamic analysis and control of an elevator system using polynomial chaos and Karhunen-Loeve approaches, *X International Conference on Structural Dynamics*, **199**, 1629–1634, (2018). https://doi.org/10.1016/j.proeng.2017.09.083

2. Zhang, H., Zhang, R. J., He, Q., et al. Variable Universe Fuzzy Control of High-Speed Elevator Horizontal Vibration Based on Firefly Algorithm and Backpropagation Fuzzy Neural Network, *IEEE Access*, **9**, 57020–57032, (2021). https://doi.org/10.1109/ACCESS.2021.3072648

3. Jiang, X. M. and Rui, Y. N. Research on vibration Control of traction elevator, *Proceedings Of the 2015 International Industrial Informatics and Computer Engineering Conference*, 2144–2147, (2015). https://doi.org/10.2991/iiicec-15.2015.466

4. Zhang, R. J., Wang, C., and Zhang, Q. Response analysis of the composite random vibration of a high-speed elevator considering the nonlinearity of guide shoe, *Journal of*

the Brazilian Society of Mechanical Sciences and Engineering, **40**(4), 190, (2018). https://doi.org/10.1007/s40430-017-0936-0

[5] Nakano, K., Hayashi, R., Suda, Y., et al. Active Vibration Control of an Elevator Car Using Two Rotary Actuators, *Journal of System Design and Dynamics*, **5**(1), 155–163, (2011). https://doi.org/10.1299/jsdd.5.155

[6] Feng, Y. H., Zhang, J. W., and Zhao Y. E. Modeling and robust control of horizontal vibrations for high-speed elevator, *Journal of Vibration and Control*, **15**, 1375–1396, (2009). https://doi.org/10.1177/1077546308096102

[7] Feng Y. H. and Zhang J. W. Study on Active Control Strategy of Horizontal Vibrations of High-speed Elevator, *Journal of system simulation*, **04**, 843–845,855, (2007).

[8] Cao, S. X., He, Q., and Zhang R. J. Robust control of high-speed elevator transverse vibration based on LMI optimization, *IOP Conference Series: Materials Science and Engineering*, **538**(1), 012032, (2019). https://doi.org/10.1088/1757-899X/538/1/012032

[9] Cao, S. X., He, Q., and Zhang, R. J. Active control strategy of high-speed elevator horizontal vibration based on LMI optimization, *Control engineering and applied informatics*, **22**(1), 72–83, (2020).

[10] Chen, C., Zhang, R. J., and Zhang, Q. Mixed H2/H-infinity guaranteed cost control for high-speed elevator active guide shoe with parametric uncertainties, *Mechanics & Industry*, **21**(5):502, (2020). https://doi.org/10.1051/meca/2020044

[11] Zhang, R. J., Qiu, T.,and Chen, C. Adaptive gain H-∞ output feedback control strategy for horizontal vibration of high-speed elevator car system based on T-S fuzzy model, *Journal of Mechanical Science and Technology*,**37**(2), 919–929, (2023). https://doi.org/10.1007/s12206-023-0132-3

[12] Chen, C., Zhang, R. J., and Zhang, Q. Finite Frequency H∞ Control for Active Guide Shoe of High-Speed Elevator with Actuator Delay, *Mechanisms and Machine Science*, **105**, 644-652, (2021). https://doi.org/10.1007/978-3-030-75793-9_62

[13] Liao, C. X. and Wei, Z. Study on Sector Capacity and Workload Model of Air Traffic Controllers Based on Least Square Method, *Proceedings of 2020 IEEE International Conference on Power, Intelligent Computing and Systems*, ICPICS 2020, 1058–1062, (2020).

[14] Wang, Y. L., Zheng, L. K., Gao, Y., and Li, S. H. Vibration Signal Extraction Based on FFT and Least Square Method, IEEE Access, **8**, 224092–224107, (2020). https://doi.org/10.1109/ACCESS.2020.3044149

[15] Santo, D. R., Balthazar, J. M., and Tusset, A. M. On nonlinear horizontal dynamics and vibrations control for high-speed elevators, *Journal of Vibration and Control*, **24**, 825–838, (2016). https://doi.org/10.1177/1077546316667324

[16] Xue, J. L., Feng, Y. H., and Wu, H. X. Study on active control of horizontal vibration for high-speed elevators based on generalized predictive PID, *Mechanical Science and Technology for Aerospace,* 1**003–8728**:08-1222-05, (2012). https://doi.org/10.13433/j.cnki.1003-8728.2012.08.037

[17] Zhang, Q., Yang, Z., Wang, C., et al. Intelligent control of active shock absorber for high-speed elevator car, *Proceedings of the Institution of Mechanical Engineers Part C-Journal of Mechanical Engineering Science*, **233**(11), 3804–3815, (2019). https://doi.org/10.1177/0954406218810045

[18] He, Q., Zhang, P., Cao, S. X., et al. Intelligent control of horizontal vibration of high-speed elevator based on gas-liquid active guide shoes, *Mechanics & Industry*, **22**, 2, (2021). https://doi.org/10.1051/meca/2020100

[19] Wang, H., Zhang, M. Q., Zhang, R. J., et al. Nonlinear predictive control of horizontal vibration of high-speed elevator, *Journal of Physics: Conference Series*, **1653**(1), 012062, (2020). https://doi.org/10.1088/1742-6596/1653/1/012062

[20] Wang, C. and Wang, X. G. Design of a Controller for Hypersonic Vehicle Based on Sliding Mode Disturbance Observer, *Electronics Optics & Control*, **27**(06), 90–94, (2020).

[21] Zhao, J. L. and Han G. X. Double Closed Loop Sliding Mode Control of Ball and Plate System Based on Particle Swarm Optimization, *Journal of Jilin Institute of Chemical Technology*,**37**(01), 63–67, (2020). https://doi.org/10.16039/j.cnki.cn22-1249.2020.01.014

[22] Xia, B. H. and Shi, X. Horizontal Vibrations of High-speed Elevator with Guide Rail Excitation, *Machinery Manufacturing & Automation*, **41**(5), 161–165, (2012). https://doi.org/10.19344/j.cnki.issn1671-5276.2012.05.053

[23] Jia, T. C., He, Q., and Zhang, R. J. Study on Linear Quadratic Regulator of High-Speed Elevator Car Horizontal Vibration Based on Genetic Algorithm Optimization. *Mechanisms and Machine Science*, **105**, 607–615, (2021). https://doi.org/10.1007/978-3-030-75793-9_58